AGU ADVANCING EARTH AND SPACE SCIENCES

Geophysical Research Letters

RESEARCH LETTER
10.1029/2024GL113734

Key Points:

- Tropospheric cooling and stratosphere warming south of 35°S are robust responses to Southern Ocean freshwater input in a multi-model ensemble
- The tropospheric cooling is driven by enhanced surface albedo in winter and colder sea surface temperature in summer
- Two types of stratospheric warming, one caused by a lowering of the tropopause and reduced water vapor content in the lower stratosphere, another by an enhanced poleward eddy heat flux

Supporting Information:

Supporting Information may be found in the online version of this article.

Correspondence to:
T. Martin,
tomartin@geomar.de

Citation:
Xu, X., Martin, T., Beadling, R. L., Liu, J., Bischof, S., Hattermann, T., et al. (2025). Robustness and mechanisms of the atmospheric response over the Southern Ocean to idealized freshwater input around Antarctica. *Geophysical Research Letters*, *52*, e2024GL113734. https://doi.org/10.1029/2024GL113734

Received 21 NOV 2024
Accepted 12 APR 2025

Author Contributions:
Conceptualization: Xiaoqi Xu, Torge Martin, Rebecca L. Beadling, Sabine Bischof
Data curation: Torge Martin, Rebecca L. Beadling, Tore Hattermann, Qian Li, Morven Muilwijk, Andrew G. Pauling, Ariaan Purich, Neil C. Swart, Max Thomas
Formal analysis: Xiaoqi Xu, Torge Martin, Jiping Liu, Sabine Bischof, Wenjuan Huo
Funding acquisition: Jiping Liu, Tore Hattermann, John C. Marshall, Inga J. Smith

Robustness and Mechanisms of the Atmospheric Response Over the Southern Ocean to Idealized Freshwater Input Around Antarctica

Xiaoqi Xu[1,2,3], Torge Martin[2], Rebecca L. Beadling[4], Jiping Liu[5], Sabine Bischof[2], Tore Hattermann[6], Wenjuan Huo[2], Qian Li[7], John C. Marshall[7,8], Morven Muilwijk[6], Andrew G. Pauling[9], Ariaan Purich[10], Inga J. Smith[9], Neil C. Swart[11], and Max Thomas[9,12]

[1]Key Laboratory of Earth System Numerical Modelling and Application, Institute of Atmospheric Physics, Chinese Academy of Sciences, Beijing, China, [2]GEOMAR Helmholtz Centre for Ocean Research Kiel, Kiel, Germany, [3]University of Chinese Academy of Sciences, Beijing, China, [4]Department of Earth and Environmental Science, Temple University, Philadelphia, PA, USA, [5]School of Atmospheric Sciences, and Southern Marine Science and Engineering Guangdong Laboratory (Zhuhai), Sun Yat-sen University, Zhuhai, China, [6]Norwegian Polar Institute, Fram Centre, Tromsø, Norway, [7]Department of Earth, Atmospheric, and Planetary Sciences, Massachusetts Institute of Technology, Cambridge, MA, USA, [8]NASA Goddard Institute for Space Studies, New York, NY, USA, [9]Department of Physics, University of Otago, Dunedin, New Zealand, [10]School of Earth, Atmosphere and Environment, ARC Special Research Initiative for Securing Antarctica's Environmental Future, Monash University, Melbourne, VIC, Australia, [11]Canadian Centre for Climate Modelling and Analysis, Environment and Climate Change Canada, Victoria, BC, Canada, [12]Met Office Hadley Center, Exeter, UK

Abstract Enhanced Antarctic ice sheet mass loss yields ocean surface freshening, cooling and sea ice expansion, which result in changes in the atmospheric conditions. Using the Southern Ocean Freshwater Input from Antarctica (SOFIA) multi-model ensemble, we study the atmospheric response to a 100-year idealized freshwater release of 0.1 Sv. All models simulate a surface-intensified tropospheric cooling and lower-stratospheric warming south of 35°S. Tropospheric cooling is attributed to sea ice expansion and the associated albedo enhancement in winter and a colder sea surface in summer. This cooling yields a downward displacement of the tropopause, reduced stratospheric water vapor content and ultimately warming around 200 hPa. An enhanced southward eddy heat flux explains warming at 10–100 hPa during austral winter. Despite a temporally (and spatially) uniform prescribed freshwater flux, a prominent sea ice seasonal cycle and atmosphere dynamics result in a distinct seasonal pattern in the occurrence and magnitude of the temperature responses.

Plain Language Summary Future accelerated melting of the Antarctic ice sheet will cause large amounts of freshwater to enter the surrounding Southern Ocean. This affects ocean and sea ice regionally and the atmosphere above. We use output from nine different climate models, all running the same experiment, to understand how the atmosphere responds to surface ocean cooling in consequence of enhanced meltwater input. Prominent changes shown by all models include cooling in the troposphere and warming in the lower stratosphere south of 35°S. Lower atmospheric temperatures are expected as the air is exposed to an expanded sea ice cover in winter and a colder ocean surface during summers. More complex mechanisms drive the warming at higher altitudes, in the lower stratosphere, where two processes dominate: Firstly, the cooling in the troposphere causes the air to contract, resulting in a lowering of the tropopause. The air above the tropopause warms due to being compressed and displaced downward. Secondly, a reduction in water vapor content reduces cooling by longwave radiation and sustains heat content in the lower stratosphere. The temperature changes also trigger dynamic responses affecting the poleward heat transport, especially during the winter season, which cause warming even higher up in the stratosphere.

1. Introduction

The rate of mass loss from the Antarctic ice sheet and its ice shelves has been increasing over the past few decades (Adusumilli et al., 2020; Smith et al., 2020) and is projected to further accelerate in the future under global warming (Naughten et al., 2023; Paolo et al., 2015). The associated freshening of the surrounding Southern Ocean (SO) has major regional to global implications (Bintanja et al., 2013; Golledge et al., 2019; Levermann

Investigation: Xiaoqi Xu, Torge Martin, Rebecca L. Beadling, Sabine Bischof, Wenjuan Huo
Methodology: Xiaoqi Xu, Torge Martin, Rebecca L. Beadling, Jiping Liu, Sabine Bischof, Tore Hattermann, Wenjuan Huo, Qian Li, John C. Marshall, Morven Muilwijk, Andrew G. Pauling, Ariaan Purich, Inga J. Smith, Neil C. Swart, Max Thomas
Project administration: Torge Martin
Supervision: Torge Martin, Jiping Liu
Visualization: Xiaoqi Xu
Writing – original draft: Xiaoqi Xu, Torge Martin
Writing – review & editing: Rebecca L. Beadling, Jiping Liu, Sabine Bischof, Tore Hattermann, Wenjuan Huo, Qian Li, John C. Marshall, Morven Muilwijk, Andrew G. Pauling, Ariaan Purich, Inga J. Smith, Neil C. Swart, Max Thomas

et al., 2020; Sadai et al., 2020; Zhu et al., 2021). However, fully interactive ice sheet/ice shelf components are lacking in most coupled climate models, increasing the uncertainty associated with future climate projections (Fyke et al., 2018; Siahaan et al., 2022; Smith et al., 2021). Numerous studies have explored the impact of freshwater perturbations from Antarctica on regional and global climate, but the patterns and magnitudes of climate responses varied widely due to different model configurations and experimental designs (Bronselaer et al., 2018; Dong et al., 2022; Fogwill et al., 2015; Pauling et al., 2016; Purich & England, 2023; Rye et al., 2020; Stouffer et al., 2007). To address this, the Southern Ocean Freshwater Input from Antarctica (SOFIA) initiative has been formed to identify robust responses and quantify the model uncertainty of such sensitivity experiments and future projections (Swart et al., 2023).

Despite model and scenario uncertainty, some consistent responses to SO freshwater perturbations have been revealed: sea surface cooling, sea ice expansion, mid-to deep ocean-warming, and a reduction of Antarctic Bottom Water formation (Bintanja et al., 2013; Chen et al., 2023; Jeong et al., 2020; Li et al., 2023). Most studies published so far have focused on ocean, sea ice and near-surface responses in general. However, Beadling et al. (2024) recently analyzed the full-depth atmospheric response to idealized Antarctic freshwater anomalies in two fully coupled climate models (GFDL-CM4 and GFDL-ESM4). Their results suggested an "opposite-global-warming" response, including surface air cooling extending to the tropopause over the subpolar SO and warming in the Upper Troposphere/Lower Stratosphere (UTLS). How robust the responses documented by Beadling et al. (2024) are and the underlying mechanisms, particularly of the warming aloft, remain unknown.

We expect Antarctic freshwater to cause responses opposite to classic global warming projections, which lack effects of ice sheet mass loss. For example, this is sea ice expansion instead of retreat. Thus, past studies investigating sea ice loss are useful references as they point out atmospheric responses to large-scale surface changes (e.g., Ayres et al., 2022; Zhu et al., 2023) only that we expect an opposite sign of the response for the freshwater release. For a seasonally varying response specifically, Ayres and Screen (2019) identified a significant warming in the stratosphere in spring (October–December) across multi-model averages, whereas England et al. (2018) found a lower stratospheric warming in autumn (March–May) and winter (June–August), but not in spring.

In this study, we use the latest results from nine fully coupled global climate models participating in the SOFIA initiative to quantify the impact of Antarctic freshwater input on the atmosphere and to access the associated model uncertainty. Our focus is on the extratropical atmospheric response over the SO and Antarctica. We address two key questions: First, is the tropospheric cooling and UTLS warming a robust response across climate models? Second, how does the atmospheric response vary seasonally and what drives the seasonality? We also suggest mechanisms governing temperature change and associated wind adjustments from the surface to the lower stratosphere.

2. Methods

2.1. Models and Experiment Design

We use output from nine climate models participating in the SOFIA initiative (Swart et al., 2023). The models chosen have provided model output for the Tier-1 *antwater* experiment, in which a 0.1 Sv ($1\ \mathrm{Sv} = 3.154 \times 10^4\ \mathrm{Gt\ yr^{-1}}$) of freshwater transport is distributed uniformly at the ocean surface layer in the nearest grid cell to the Antarctic coast at a constant rate for 100 model years: FOCI (Matthes et al., 2020), HadGEM3-GC3.1-LL (Kuhlbrodt et al., 2018), CESM2 (Danabasoglu et al., 2020), ACCESS-ESM1-5 (Ziehn et al., 2020), GISS-E2-1-G (Kelley et al., 2020), NorESM2-MM (Seland et al., 2020), CanESM5 (Swart et al., 2019), GFDL-ESM4 (Dunne et al., 2020) and GFDL-CM4 (Held et al., 2019). We include *antwater* ensemble members where available (ensemble size varies from 3 to 10, see Table S1 in Supporting Information S1). The FOCI model is used for extended analysis. It consists of the NEMO-LIM model components for ocean and sea ice applied to a regular grid of 0.5° horizontal resolution and 46 vertical ocean levels, which are coupled to the ECHAM-JSBACH atmosphere and land models run with 1.8° horizontal resolution and 95 vertical atmosphere levels extending up to 0.01 hPa grids (for details see the Supporting Information S1). Tier-1 experiments are conducted under pre-industrial control forcing (*piControl*) as defined by the CMIP6 protocol (Eyring et al., 2016). Further details are provided in the Supporting Information (Text S1 in Supporting Information S1).

2.2. Analysis of Model Output

The analysis of air temperature and zonal wind is based on monthly mean output. We refer to the *piControl* and *antwater* simulations as "CTRL" and "ANT," and to the difference of *antwater* minus *piControl* results as "response" to the freshwater input. For the latter, we average the last 50 years of ANT and 500 years of CTRL (where available, 100 years otherwise; see Table S1 in Supporting Information S1). CTRL is in equilibrium without relevant trends in any of the quantities analyzed. ANT is considered to be in quasi-equilibrium after 50 years for ocean surface and atmosphere conditions, where the quasi-equilibrium state is defined based on time series of averages across the SO (40°S–70°S). In this region and for the second half of ANT, the annual mean sea surface temperature, surface air temperature, and sea ice coverage show small interannual variations and no significant trends (see Figure S1 in Supporting Information S1). Atmospheric quantities adjust more rapidly and are assumed to have fully diverged from CTRL where differences are significant. Identifying the underlying processes governing the atmospheric temperature response in the stratosphere requires daily model output not available from most participating models. Thus, we supplement the analysis with additional daily atmosphere-model output from FOCI, providing context to the potential mechanisms behind the ensemble response.

Upward planetary wave propagation is a process by which lower tropospheric anomalies can affect the stratosphere. To estimate its effect on the temperature response, we use the eddy heat flux at 50 hPa averaged over 45°–75°S (Inness et al., 2020; Newman et al., 2001; Polvani & Waugh, 2004). The eddy heat flux is proportional to the vertical component of the Eliassen-Palm flux, which describes the amount of upward propagating planetary waves into the lower stratosphere (Newman et al., 2001; Randel et al., 2002). For the analysis of eddy heat flux:

$$[v'T'] = \{[(v-[v]) * (T-[T])]\}|_{45^\circ-75^\circ S}$$

where [] denotes the zonal mean and { } is the meridional mean limited to 45°–75°S, daily fields of temperature T and meridional wind v are required. Newman et al. (2001) demonstrated that temperatures in the lower stratosphere on a given day are correlated with the eddy heat flux over several weeks prior, rather than with instantaneous upward wave activity. Following Inness et al. (2020), we use a 45-day running mean centered on the last day of this period.

For indicating statistical significance of the multi-model mean results in Figures 1 and 2, we use hatching to indicate the number of models that have significant responses. For each model, significance is tested using a Student's t-test comparing the response in ANT to internal variability in CTRL. For example, the sample of FOCI for ANT consists of eight ensemble members from which only the last 50 years are considered yielding a total sample size of 400 years. The reference sample simply consists of 500 years of CTRL. A two-sided t-test for unequal variances is applied to the two samples and counted as 1 (null-hypothesis of equal mean rejected) when exceeding the 95% confidence level. This is depicted as stippling in Figures 1c, 1d, 2c, and 2d for FOCI. After repeating this for all models, the total of these counts is illustrated in Figures 1a, 1b, 2a, and 2b using different hatching.

3. Results

3.1. Robustness of Multi-Model Ensemble Responses

In response to the freshwater applied around the Antarctic margins, all models simulate surface ocean cooling, expansion of sea ice and near-surface atmosphere cooling across the SO (Figure S1 in Supporting Information S1), consistent with previous freshwater studies (e.g., Bronselaer et al., 2018; Pauling et al., 2016; Rye et al., 2020). Figure 1a shows the multi-model annual mean vertical distribution of air temperature anomalies resulting from the freshwater release into the SO. The response to an increased Antarctic sea ice extent and ocean surface cooling results in global atmospheric impacts, including troposphere-wide cooling and an approximately anti-symmetric pattern in the lower stratosphere, characterized by warming over the mid-to high-latitudes and cooling over the low-latitudes. The changes are most pronounced in the Southern Hemisphere, where the largest cooling exceeds 1°C near the surface over Antarctica and the SO. The cold anomalies extending throughout the troposphere up to 330 hPa are statistically significant across all models. Sea ice expansion is another consequence of freshwater input and cooling. This trend is the opposite to typical global warming simulations showing sea ice retreat. Accordingly, we find atmospheric responses that have similar patterns but with differences to the control

10.1029/2024GL113734

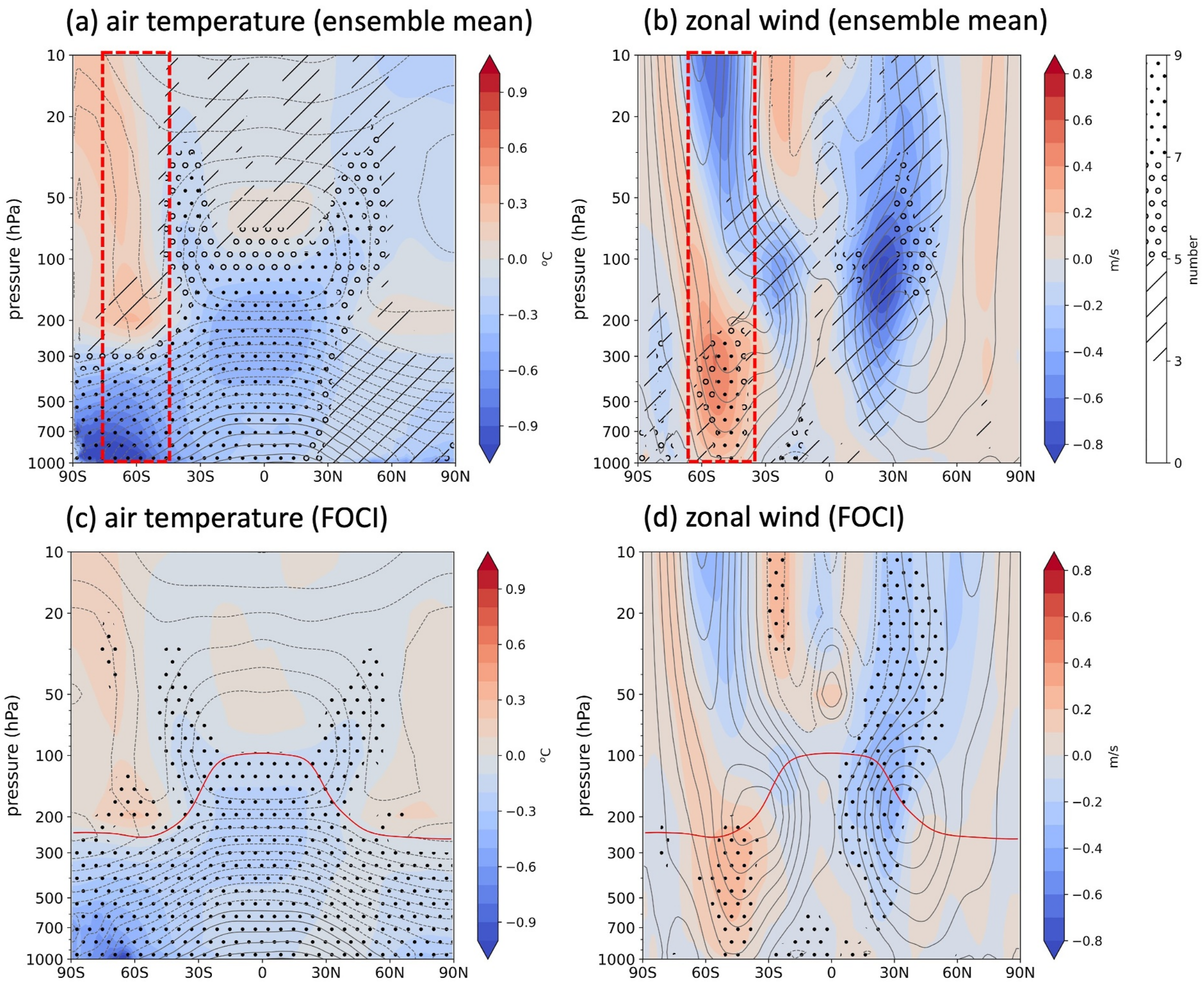

Figure 1. Vertical distribution of annual mean (a) air temperature and (b) zonal wind response of the multi-model ensemble (shading; *antwater* minus *piControl*). Gray contours show the CTRL multi-model mean with contour intervals of 5°C for temperature and 5 ms^{-1} for zonal wind, negative values are shown as dashed lines. Stippling/hatching in panels (a) and (b) represent the number of models which have a statistically significant response at the 95% confidence level for student's *t*-test at that location. The red-dashed boxes indicate the regions for spatial averaging in further analysis (a) 45°–75°S; (b) 35°–65°S, (c)–(d) are the same as panels (a)–(b) but for the FOCI model only; the red line denotes the tropopause height diagnosed by FOCI following the World Meteorological Organization (WMO, 1957) definition; here stippling denotes a statistically significant response at the 95% confidence level for student's *t*-test.

state of opposite sign—and different magnitude—compared to changes in global warming simulations. For example, the vertical structure of the atmospheric cooling shows a bullhorn-like zonal-mean pattern between 30°S and 30°N (300–20 hPa) with a core at 400–150 hPa (Figure 1a). The same structure appears in global warming scenarios under increased CO_2 but as warming (Huang et al., 2016, their Figure 2). The same warming pattern can be triggered by perturbing sea ice conditions directly (e.g., albedo reduction) forcing a loss of ice area (Ayres et al., 2022; England et al., 2020). In this regard, we confirm earlier findings and conclude, that the freshwater perturbation forces the atmospheric response through altered sea ice coverage and that sea ice gain/loss on an SO-wide scale can drive cooling/warming as remotely as the tropical lower stratosphere.

Associated with the temperature response, zonal wind changes (Figure 1b) are only statistically significant in most models over the subpolar SO (35°S–65°S, red box). In this region, the westerlies, which are associated with the tropospheric jet stream, strengthen on the southern flank with the maximum response observed at 500–300 hPa. In contrast, there is a significant local warming above the tropopause at around 200 hPa south of 60°S (~0.4–0.5°C) extending through the Upper Troposphere/Lower Stratosphere (UTLS) region and to a lesser degree (<0.2°C) in the tropics above 80 hPa (Figure 1a). While a weakening of the stratospheric polar vortex occurs in the Southern Hemisphere, it is not significant (Figure 1b).

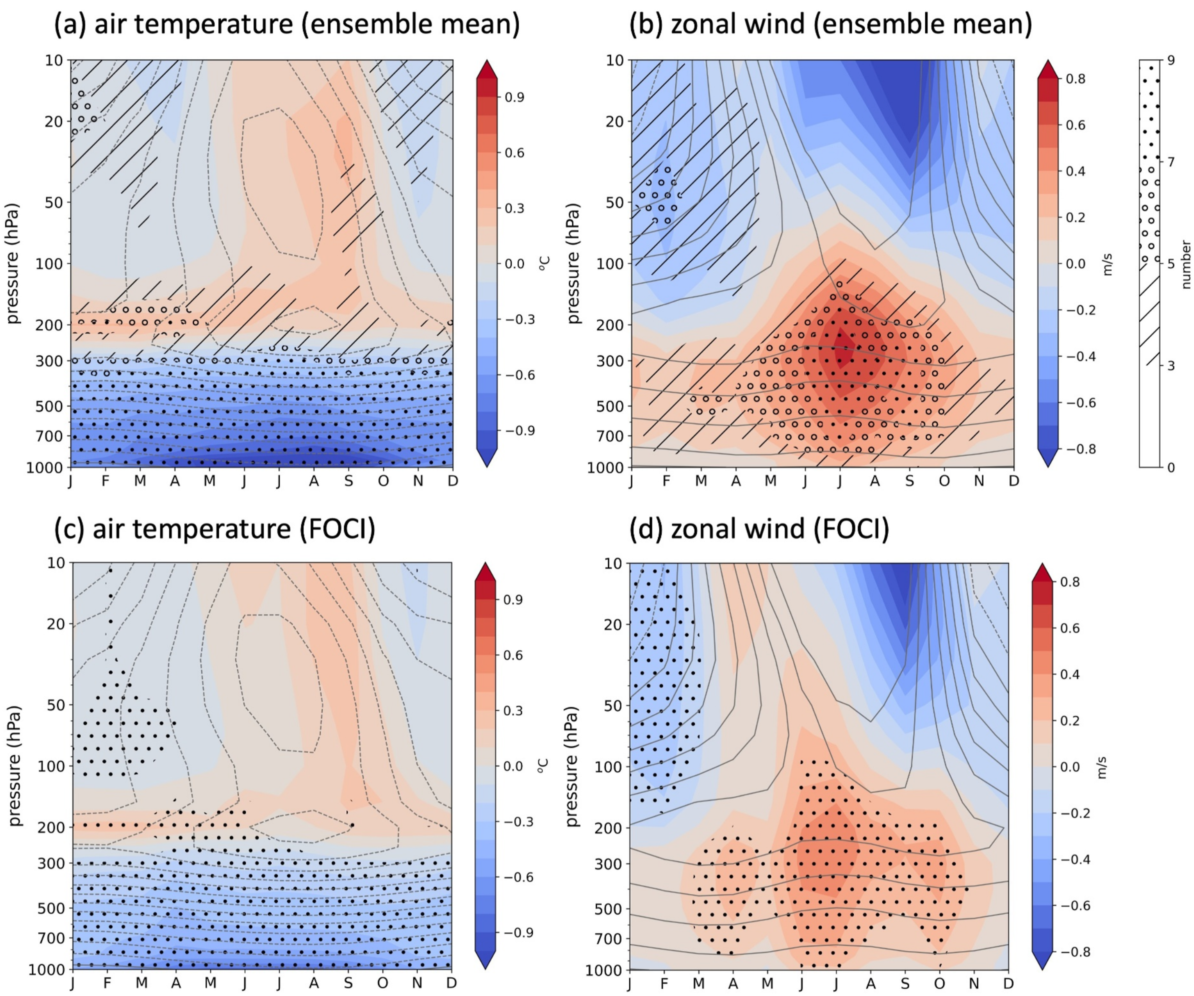

Figure 2. Seasonal cycle of area-averaged vertical distribution of panel (a) air temperature between 45°S and 75°S and (b) zonal wind response between 35°S and 65°S, (shading; *antwater* minus *piControl*). Gray contours depict the CTRL climatology of the multi-model mean; the contour interval is 5°C for temperature and 5 $m \cdot s^{-1}$ for zonal wind, with negative values shaded. Stippling/hatching in panels (a)–(b) represent the number of models with a statistically significant response at the 95% confidence for student's *t*-test level at each location. (c)–(d) are the same as panels (a)–(b) but for the output from FOCI; here, stippling indicates a statistically significant response at the 95% confidence level.

Many individual response patterns share features with the ensemble mean, particularly in the temperature structure (Figure S2 in Supporting Information S1). While the cooling of the troposphere is robust across all models, although the magnitudes vary. The warming in the stratosphere over Antarctica is also present in all models, though it is statistically significant in only four of them (FOCI, HadGEM3-GC3.1-LL, CESM2, ACCESS-ESM-1-5; see Figure 1c and Figure S2 in Supporting Information S1). Only some models show a weak warming response in the Arctic tropopause region (FOCI, HadGEM3-GC3.1-LL, CESM2, ACCESS-ESM-1-5, NorESM2-MM, CanESM5; see Figure 1c and Figure S2 in Supporting Information S1).

Compared to temperature, the zonal wind response is less consistent across models. For example, the significant strengthening of the Southern Hemisphere westerlies is confined to below 200 hPa in most models (i.e., FOCI, HadGEM3-GC3.1-LL, CESM2, ACCESS-ESM-1-5, GFDL-ESM4, GFDL-CM4; see Figure 1d and Figure S2 in Supporting Information S1), while it extends throughout the troposphere and even into the stratosphere in CanESM5 and GISS-E2-1-G. The relationship between changes in air temperature and zonal wind can be partly explained by thermal wind balance, that is, changes in the meridional temperature gradient resulting in changes in zonal velocities. Previous studies suggest that the shift in the Southern Hemisphere jet observed in response to rising greenhouse gas concentrations is linked to changes in large-scale meridional temperature gradients, affecting the jet's position and strength (Bracegirdle et al., 2018; Grise & Polvani, 2017; Wood et al., 2021).

Although the magnitude of the changes in temperature and wind in FOCI are only half of those of the multi-model mean, the patterns in FOCI are consistent with the multi-model mean (Figures 1c and 1d).

The seasonal variation of the air temperature response over the SO and Antarctica (red-dashed box in Figure 1a) shows a persistent cooling and increase in zonal wind strength in the troposphere throughout the year (Figure 2a). In the troposphere, the largest signal occurs in austral fall and winter (April–September), which is attributed to the freshwater-induced sea ice expansion during the freezing period. The presence of sea ice reduces the local air-sea heat exchange and increases the surface albedo, both of which drive local cooling of the near-surface atmosphere. There is a strengthening of westerlies extending to 100 hPa in the austral winter (June–September), with the largest signal occurring around 300 hPa (Figure 2b). In the UTLS, warming at 200 hPa is sustained year-round, reaching a peak magnitude during the austral summer (January–March). This warming response is also observed extending from 200 hPa upward to 10 hPa during winter to early spring (Figure 2a; June–October), maximizing in September. This is accompanied by a weakening of the stratospheric polar vortex, though the effect is not statistically significant (Figure 2b). These seasonal variations are consistent with the results of previous sea-ice-loss studies: the largest difference in surface air temperature occurs in austral autumn and winter (March–August), while the temperature changes in the lower stratosphere are more pronounced in winter and spring (June–November) (Ayres et al., 2022, their Figures 3 and 8).

Compared to the annual mean, the seasonal cycle exhibits greater inter-model spread. The strong cooling in the troposphere accompanied by weak warming in the upper troposphere is a robust feature, whereas models diverge in the timing, vertical distribution and magnitude of the warming extending to the stratosphere (Figure S3 in Supporting Information S1). From the individual model results, we can see that a strengthening of the westerlies generally coincides with a strong cooling response. The high-level warming persists for 3–5 months, except for two models in which a cooling and strengthening of the polar vortex is present in August (ACCESS-ESM-1-5, NorESM2-MM; Figure S3 in Supporting Information S1).

3.2. Mechanisms of Temperature Change

In this section, we explore the mechanisms behind the three major patterns of air temperature response over the SO and Antarctica: cooling at the surface, year-round warming at 200 hPa and wintertime warming at 50 hPa. As motivated above, we focus this analysis on FOCI only, for which we have the appropriate diagnostics and which yields response generally representative of the multi-model ensemble.

The seasonal variability of surface air temperature is stronger than that of sea surface temperature (SST) in high latitudes because of the pronounced seasonal cycle of sea ice coverage (see Figure S4 in Supporting Information S1). Near-surface air cooling occurs throughout the year with the largest magnitude in austral winter. The seasonality is strongly influenced by radiation and heat exchange between sea ice/ocean and the atmosphere. Thus, we analyze changes in the surface net heat flux (NHF) and its individual components by season: latent (LHF) and sensible heat fluxes (SHF), surface net shortwave (SWR) and surface net longwave radiation (LWR). Figure 3 shows maps of SST change along with the most prominent heat flux changes in austral summer and winter, where positive values indicate heat gain for the ocean (i.e., heat loss from the atmosphere). All fields for all seasons are displayed in Figure S5 in Supporting Information S1.

As the Antarctic freshwater spreads across the SO, it enhances near-surface stratification, reducing mixed layer depth (Pauling et al., 2016) and causing a large-scale reduction in SST (Bintanja et al., 2013; Bronselaer et al., 2018; Kirkman & Bitz, 2011). The ice-free SO is dominated by a positive downward surface NHF response at 40°–50°S, which is particularly strong in the Atlantic and Indian sectors in all seasons (Figures 3b and 3f). An exceptional opposite response is present in the Malvinas (40°–45°S, 30°–60°W) and Agulhas (35°–40°S, 0°–35°E) regions—and of weaker magnitude in the Pacific sector. The similarity of the spatial patterns of SAT, NHF and LHF suggest that surface ocean cooling is dampened by downward LHF (Figures 3a–3c and 3e–3g). In other words, ocean-driven surface cooling leads to a reduction in evaporation (anomalous downward LHF), which dominates LHF in CTRL at these latitudes (upward LHF), providing negative feedback to dampen the ocean cooling. Along with SHF this is the dominant mechanism by which the ocean forces a wide-spread surface-intensified tropospheric cooling in the sea-ice free latitudes of the SO.

In the ice-covered ocean south of 50°S, the response differs significantly between austral spring/summer and fall/winter seasons. We here focus on the stark contrast of summer (SON) and winter (DJF) for explaining the

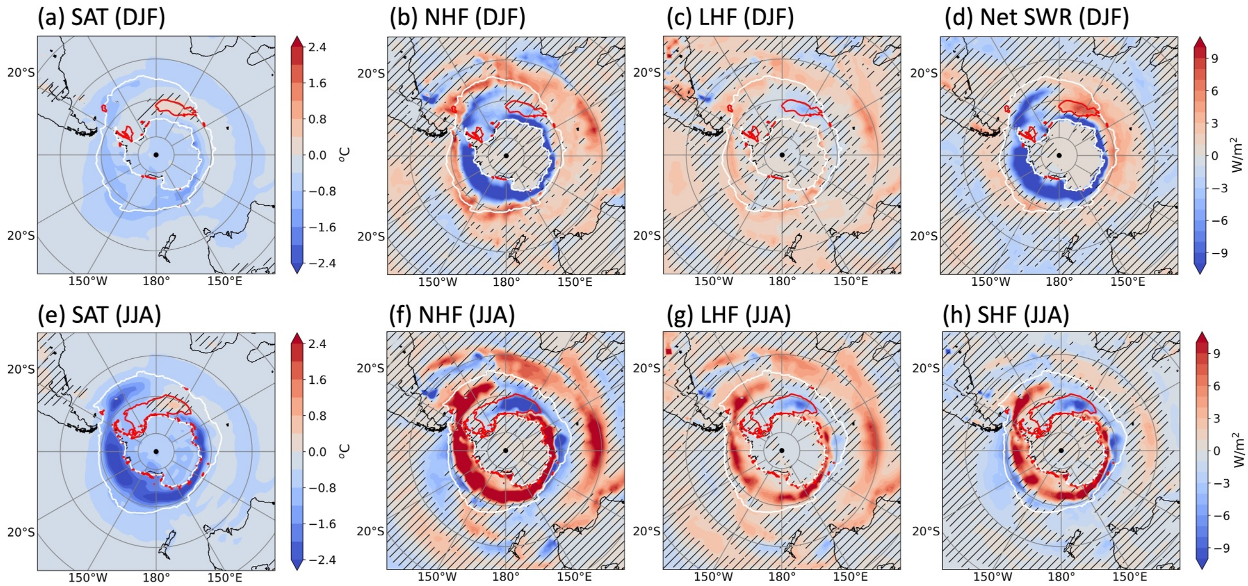

Figure 3. Seasonal mean heat flux and radiation responses derived from FOCI: (a) surface air temperature (SAT), (b) surface net heat flux (NHF), (c) latent heat flux (LHF) and (d) surface net shortwave radiation (SWR) in austral summer (December-February); (e) SAT, (f) surface NHF, (g) LHF and (h) sensible heat flux (SHF) in austral winter (June–August). Positive values indicate a downward heat flux into the ocean. Stippling denotes a statistically significant response at the 95% confidence level for student's *t*-test. Sea ice concentration (SIC) is generally increasing, and the white contour depicts the ice extent in ANT; only in areas enclosed by red contours, SIC is decreased in ANT compared to CTRL.

differences. Since the key processes also affect the shoulder seasons (SON and MAM), we display all seasons in Figures S4 and S5 in Supporting Information S1. The seasonality of solar insolation at polar latitudes and sea ice coverage are major drivers of the differences, which are prominently visible in the heat flux components displayed in Figure 3, where positive values indicate heat gain for the ocean (i.e., heat loss from the atmosphere) and the white outline depicts the ensemble mean sea ice edge in ANT. During summer, the region with increased sea ice concentration (SIC, Figure S4 in Supporting Information S1) exhibits a strong upward NHF response. This is attributed to a substantial upward net SWR anomaly (Figure 3d), due to enhanced surface albedo by presence of sea ice. The net radiation at the top of the atmosphere (TOA) indicates that a significant portion of the reflected solar radiation is emitted back into space (Figure S4 in Supporting Information S1). In contrast, a strong downward NHF response dominates the same region in austral winter (Figure 3f). We find both LHF and SHF contributing (Figures 3g and 3h), which is related to increased SIC, too. Specifically, the more compact and thicker sea ice inhibits turbulent heat loss to the atmosphere, thereby contributing to tropospheric cooling. LHF and SHF contribute the dominant changes to an altered NHF, whereas the share of net LWR is comparatively small (Figure S5 in Supporting Information S1). The observed downward net LWR response around Antarctica can be attributed to an increase in cloud cover, predominantly low clouds, which generally intensifies over the subpolar to mid-latitude SO (cf. Total cloud cover (TCC) in Figure S4 in Supporting Information S1 and Net LHF in Figure S5 in Supporting Information S1).

In the Weddell Sea there is a larger area showing a decrease in SIC (enclosed by the red contour in Figure 3), which is caused by open ocean deep convection occurring in the eastern Weddell Gyre (0°–40°E) in three out of eight FOCI ANT members but not in CTRL. Open-ocean deep convection brings warm deep waters to the surface reducing SIC and warming SST (Figure S4 in Supporting Information S1). While open-ocean deep convection is typically diminished by freshwater release in the SOFIA multi-model ensemble (Chen et al., 2023), this is different in FOCI. In this model, warming at mid-depth, which matches the response seen in other models, can overcome a subtle increase in the stratification of the top 200 m of the Weddell Gyre under favorable wind and sea ice conditions as the freshwater released along the coast is largely exported with the outer gyre circulation (details are subject to a companion study). Here, we use this as an opportunity to showcase that SIC reduction causes the exact opposite responses as outlined in the previous paragraph. We emphasize that the anomalies caused by the deep convection are regionally confined and do not affect the results outside this region, where no major

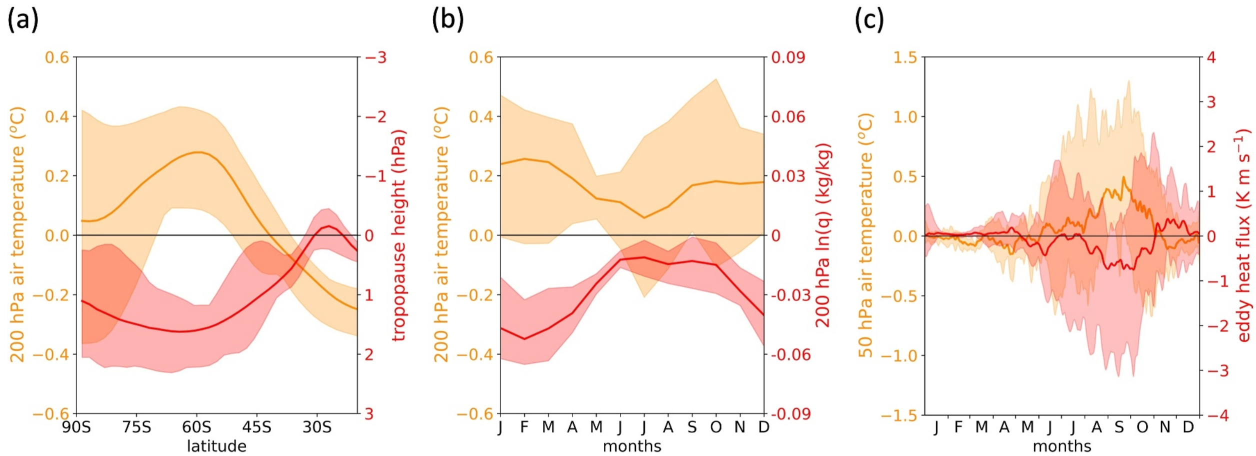

Figure 4. (a) Annual mean response of zonally averaged air temperature at 200 hPa (orange) and tropopause height (red) as diagnosed by FOCI following the World Meteorological Organization (WMO, 1957) standard. (b) Monthly mean response of air temperature (orange) and the natural logarithm of specific humidity (*ln (q)*; red) both at 200 hPa averaged over 45°–75°S. (c) Daily mean response of air temperature (orange) and total eddy heat flux (red) both at 50 hPa averaged over 45°–75°S. Mean eddy heat flux is an average of the 45-day period prior to the given day. The solid lines indicate the FOCI ensemble mean and the shading the range of the eight individual ensemble members in FOCI.

differences between the full eight member and reduced non-convecting five-member ensemble mean were found (not shown).

The warming response in the UTLS over the SO, particularly at 200 hPa, is present year-round (Figure 2c). Figure 4a (orange line) shows that the warming of the zonally averaged air temperature at 200 hPa is confined to the region south of 45°S, with a maximum of 0.28 ± 0.09°C located around 60°S (orange line). This is associated with a downward displacement of the tropopause by up to 1.62 ± 0.38 hPa (red line in Figure 4a). The tropopause height is computed following the WMO (WMO, 1957) standard as implemented in the ECHAM model, FOCI's atmospheric component. Previous studies revealed that the increase in tropospheric temperature decreases the static stability in the region of the tropopause and raises tropopause height (Lorenz & DeWeaver, 2007; Santer et al., 2003). Conversely, a decrease in tropospheric temperature results in a reduction of tropopause height. This implies a thinning of the troposphere which is associated with the wide-spread cooling in the troposphere and a warming in the UTLS.

Additionally, water vapor plays a critical role in regulating air temperature. Even minor fluctuations in water vapor within the UTLS can lead to significant changes in radiative balance and potentially affect the climate (Charlesworth et al., 2023; Forster & Shine, 1999; Maycock et al., 2013). Figure 4b demonstrates the covarying seasonal evolution of area-averaged air temperature at 200 hPa and specific humidity, *ln(q)*. Though the warming response at 200 hPa is present year-round, it displays a slight seasonal variation, being more pronounced during the warmer months of January to March, during which the response in water vapor is also notably stronger (Figure S6 in Supporting Information S1). The mechanism by which stratospheric water vapor affects temperature is analogous to the mechanism described for classic global warming experiments but with opposite sign (Banerjee et al., 2019; Dessler et al., 2013; Wang & Huang, 2020): The widespread cooling in the troposphere favors a reduced water vapor content, which subsequently leads to less water vapor entering the UTLS region. A decrease in UTLS water vapor reduces stratospheric emissivity. This results in less longwave radiation being emitted upward into upper layer or downward into the troposphere, thereby warming the UTLS. Although less water vapor will also decrease the absorption of shortwave radiation, this effect is much weaker than the longwave effect.

In contrast, the temperature response in the stratosphere above 100 hPa exhibits more seasonal variation, with the main warming occurring primarily during austral winter and spring. We focus on 50 hPa at which FOCI and the other eight models show a strong signal (Figure 2a). The zonal-mean eddy heat flux is the fundamental diagnostic for estimating the activity of waves propagating from the troposphere into the stratosphere. In the Southern Hemisphere, the climatological eddy heat flux is always negative, and a larger absolute value means stronger upward wave propagation (Inness et al., 2020; Newman & Nash, 2000). The temperature in the lower stratosphere

10.1029/2024GL113734

at a given date is related to the time-integrated eddy heat flux over several weeks prior to that date (Inness et al., 2020; Newman et al., 2001; Polvani & Waugh, 2004). The maximum anomaly of eddy heat flux response to freshwater release (at 50 hPa averaged over 45 days prior to the temperature date) occurs from June to October, which is consistent with the temperature response at this altitude (Figure 4c). The subsequent reversed, positive anomalies of the eddy heat flux also match the cold temperature anomalies in November. Our experiments show that a freshwater perturbation at high southern latitudes may also affect the coupling process between the troposphere and stratosphere, reflected in the enhanced eddy heat flux. We conclude that this very likely explains the seasonal warming signal in the lower stratosphere.

4. Discussion and Conclusions

In this study, we demonstrate robustness in the atmospheric response to idealized freshwater input around Antarctica across nine climate models. Robust features are a strong tropospheric cooling and weak tropopause warming south of 35°S, accompanied by a strengthening of the jet stream and a weakening of the stratospheric polar vortex. These responses are opposite in sign but similar in pattern to those already known from global warming projections lacking the feedback of an interactive Antarctic ice sheet (Ayres et al., 2022; Ayres & Screen, 2019; England et al., 2018; Zhu et al., 2023) and hence have the potential to mitigate or delay climate change to some extent. An analysis of the seasonality reveals two types of stratospheric warming: a year-round at 200 hPa and a seasonal in the lower stratosphere between 10 and 100 hPa during August to October. We suggest that the year-round cooling in the troposphere is induced by SST cooling in the open ocean, dampened turbulent heat flux and enhanced reflection of SWR from the expanded sea ice cover. This tropospheric cooling leads to a downward displacement of the tropopause and a decrease in water vapor content, resulting in less LWR emission, which explains the warming in the UTLS. Additionally, an increased southward eddy heat flux is responsible for the observed austral winter and early spring warming in the stratosphere above 100 hPa.

Our study demonstrates that previously reported results, in particular those of Beadling et al. (2024), are robust across a suite of models and provides evidence for mechanisms governing the magnitude, pattern and seasonal timing of the temperature response in the troposphere and stratosphere. We expand previous findings in showing that the lower stratospheric warming features strong seasonality and only occurs in austral winter and spring. The analysis of eddy heat flux corroborates the current understanding of lower stratospheric warming to be closely linked to enhanced upward wave propagation from the troposphere. While good agreement is found to the temperature response, the changes of the westerly winds exhibit larger spread across models. We emphasize that the SO surface cooling/warming and associated sea ice advance/retreat yield responses of similar patterns but opposite sign, meaning that different processes triggered by global warming may cancel each other's consequences—at least for a while—and thus evolve undetected. The SO cooling caused by enhanced Antarctic meltwater input is not represented in the models participating in phases 5 and 6 of the Coupled Model Intercomparison Project (CMIP5 and CMIP6) (Bracegirdle et al., 2020; Dong et al., 2022; Kang et al., 2023; Pauling et al., 2016; Rye et al., 2020). Overall, our findings advocate once more for including the response of the Antarctic ice sheet and ice shelves to global warming in future climate projections as their non-linear feedbacks are complex and significant.

So far, only a few studies have documented the atmospheric response to freshwater release from Antarctica and even fewer have addressed the associated seasonality. However, since sea ice expansion is a first-order response, we can compare with earlier studies of large-scale Antarctic sea ice change. For example, the projected sea ice loss under global warming (notably based on scenarios lacking fluxes from melting ice sheets) will result in surface warming and tropopause cooling, along with opposing wind change patterns (e.g., England et al., 2018). The seasonal timing of this response differs for atmosphere-only and coupled climate model experiments (Ayres & Screen, 2019; England et al., 2018), as demonstrated by Smith et al. (2017). Uncertainty is larger for the associated dynamic response, that is, change in zonal winds, as inter-model spread is larger and links to temperature inconclusive.

We propose the decreased water vapor content to play a role in the UTLS warming. The water vapor response is primarily confined to the UTLS and troposphere (south of 50°S and below 100 hPa) throughout all seasons (Figure S6 in Supporting Information S1). While not being the only driver of the UTLS warming, water vapor and stratospheric temperature covariance merits further discussion. Previous studies have identified the extratropical lowermost stratosphere as the most critical region for stratospheric water vapor radiative perturbation (Banerjee et al., 2019; Dessler et al., 2013). Water vapor content in the troposphere is reduced due to both, decreased evaporation at the surface (Figure S6 in Supporting Information S1) and colder air containing less water vapor. This has implications for the stratosphere. The Brewer-Dobson Circulation is a key process in transporting water vapor from tropics to the high latitudes within stratosphere. Studies show that a stronger circulation enhances updrafts in the tropics, which leads to an enhanced transport of water vapor into the stratosphere under global warming conditions (Poshyvailo-Strube et al., 2022; Wang & Huang, 2020). Conversely, cooling in the troposphere from Antarctic freshwater input may weaken the Brewer-Dobson Circulation, reducing water vapor transport into the polar stratosphere from an already water vapor diminished troposphere. A strong polar vortex, polar stratospheric temperatures below 195 K and elevated levels of water vapor favor the development of the ozone hole (Holton et al., 1995; Shindell, 2001; Solomon, 1999). In addition, recent research showed that sudden stratospheric warming events enhance Antarctic ozone levels (Safieddine et al., 2020; Stolarski et al., 2005). The overlapping effects of ozone hole recovery, Antarctic ice sheet melting and greenhouse gas forcing on stratospheric temperature are an intriguing topic that needs further study.

In accordance with earlier studies of Antarctic freshwater release (e.g., Bronselaer et al., 2018; Park & Latif, 2019) the SOFIA simulations show an atmospheric response outside the SO region extending far into the northern hemisphere, such as a weakening of the jet stream on its equatorward flank in both hemispheres. Such teleconnections are highly important for understanding Antarctica's influence on the global climate. The increased freshwater input resulting in the SO surface cooling may also result in global-scale phenomena such as a northward shift of the Inner-Tropical Convergence Zone (Bronselaer et al., 2018), cooler conditions in the eastern tropical Pacific (Kang et al., 2023), a delay in the future weakening of Atlantic Meridional Overturning Circulation strength, which enhances northward heat transport (Sadai et al., 2020), and a reduction in the global warming rate (Bronselaer et al., 2018; Dong et al., 2022). Despite being an idealized scenario, the simulations presented here yield unique evidence of what must be considered robust patterns of climate change in response to enhanced Antarctic ice sheet mass loss. Since most of these responses act opposingly to global warming mechanisms diagnosed from model experiments lacking Antarctic freshwater, our results support the notion of a potential delay of anthropogenic climate change through the SO processes (Bronselaer et al., 2018; Dong et al., 2022; Li et al., 2024; Purich & England, 2023).

Data Availability Statement

The data of the freshwater experiments are made available by the SOFIA initiative (https://sofiamip.github.io/data-access.html; Swart et al., 2023), the *piControl* simulations through the common CMIP6 archive (Eyring et al., 2016). Jupyter notebooks and processed data needed to re-produce the analysis and figures of this study are available through GEOMAR at https://hdl.handle.net/20.500.12085/3351529c-687e-4ac5-bf64-0ce903acf797 (Martin & Xu, 2024). The original model output can be accessed at https://crd-data-donnees-rdc.ec.gc.ca/CCCMA/SOFIA/ (last access: 22 Apr 2025). We request that the experimental design paper Swart et al. (2023) should be cited whenever the SOFIA data are used in publication. Please contact SOFIA at https://sofiamip.github.io/ (last access: 22 Apr 2025).

Acknowledgments

The authors thank two anonymous reviewers for their thorough reviews and constructive comments helping to improve the manuscript. This research is supported by the National Key R&D Program of China (2024YFF0506600) and the Southern Marine Science and Engineering Guangdong Laboratory (Zhuhai) (SML2024SP023). XX and JL acknowledge the support from Training Program Scholarship by the University of Chinese Academy of Sciences. TM received funding from the German Federal Ministry of Education and Research (BMBF) through project PalMod: From the Last Interglacial to the Anthropocene--Modelling a Complete Glacial Cycle, WP1.4.3 (FZK:01LP1918C). The required computational resources for running FOCI were supported by the Alliance for National High Performance Computing (Nationales Hochleistungsrechnen—NHR) using the facility of the Zuse Institute Berlin (ZIB), Germany. RLB acknowledges support from NSF Division of Polar Programs Grant NSF2319828. TH acknowledges support from the Research Council of Norway through its Centers of Excellence funding scheme via iC3: Centre for ice, Cryosphere, Carbon and Climate (project number 332635), and the NorESM simulations are supported by Sigma2 HPC, Norway, project NN9824K. MM received funding from the European Union's Horizon 2020 Research and Innovation Programme (Grant 101003826) via project CRiceS. AGP, IJS and MT were supported by the New Zealand Deep South National Science Challenge (MBIE contract number C01X1412) and the New Zealand Antarctic Science Platform (University of Otago subcontract 19424 from VUW's ASP Project 4 contract with Antarctica New Zealand through MBIE SSIF Programmes Investment contract number ANTA1801). They wish to acknowledge the use of New Zealand eScience Infrastructure (NeSI) high performance computing facilities, consulting support and/or training services as part of this research. New Zealand's national facilities are provided by NeSI and funded jointly by NeSI's collaborator institutions and through the Ministry of Business, Innovation & Employment's Research Infrastructure programme. URL: \url{https://www.nesi.org.nz}. They would like to acknowledge high-performance computing support from Cheyenne (https://doi.org/10.5065/D6RX99HX) provided by NCAR's Computational and Information Systems Laboratory, sponsored by the National Science Foundation. They also thank the Community Earth System Model (CESM) Polar Climate Working Group and the CESM Climate Variability and Change Working Group for computing time on the Cheyenne supercomputer. AP was supported by ARC SRIEAS Grant SR200100005 Securing Antarctica's

References

Adusumilli, S., Fricker, H. A., Medley, B., Padman, L., & Siegfried, M. R. (2020). Interannual variations in meltwater input to the Southern Ocean from Antarctic ice shelves. *Nature Geoscience*, *13*(8), 616–620. https://doi.org/10.1038/s41561-020-0616-z

Ayres, H. C., & Screen, J. A. (2019). Multimodel analysis of the atmospheric response to Antarctic sea ice loss at quadrupled CO2. *Geophysical Research Letters*, *46*(16), 9861–9869. https://doi.org/10.1029/2019GL083653

Ayres, H. C., Screen, J. A., Blockley, E. W., & Bracegirdle, T. J. (2022). The coupled atmosphere–ocean response to Antarctic sea ice loss. *Journal of Climate*, *35*(14), 4665–4685. https://doi.org/10.1175/JCLI-D-21-0918.1

Banerjee, A., Chiodo, G., Previdi, M., Ponater, M., Conley, A. J., & Polvani, L. M. (2019). Stratospheric water vapor: An important climate feedback. *Climate Dynamics*, *53*(3–4), 1697–1710. https://doi.org/10.1007/s00382-019-04721-4

Beadling, R. L., Lin, P., Krasting, J., Ellinger, W., Coomans, A., Milward, J., et al. (2024). From the surface to the stratosphere: Large-scale atmospheric response to Antarctic meltwater. *Geophysical Research Letters*, *51*(21), e2024GL110157. https://doi.org/10.1029/2024GL110157

Bintanja, R., van Oldenborgh, G., Drijfhout, S., Wouters, B., & Katsman, C. (2013). Important role for ocean warming and increased ice-shelf melt in Antarctic sea-ice expansion. *Nature Geoscience*, *6*(5), 376–379. https://doi.org/10.1038/ngeo1767

Bracegirdle, T. J., Hyder, P., & Holmes, C. R. (2018). CMIP5 diversity in southern westerly jet projections related to historical sea ice area: Strong link to strengthening and weak link to shift. *Journal of Climate*, *31*(1), 195–211. https://doi.org/10.1175/JCLI-D-17-0320.1

Bracegirdle, T. J., Krinner, G., Tonelli, M., Haumann, F. A., Naughten, K. A., Rackow, T., et al. (2020). Twenty first century changes in Antarctic and Southern Ocean surface climate in CMIP6. *Atmospheric Science Letters*, *21*(9), e984. https://doi.org/10.1002/asl.984

Bronselaer, B., Winton, M., Griffies, S. M., Hurlin, W. J., Rodgers, K. B., Sergienko, O. V., et al. (2018). Change in future climate due to Antarctic meltwater. *Nature*, *564*(7734), 53–58. https://doi.org/10.1038/s41586-018-0712-z

Environmental Future. QL and JM are supported by the NASA MAP program 19-MAP19-0011 and the MIT-GISS cooperative agreement. The model simulations and analysis were conducted on the NASA High-End Computing (HEC) Program through the NASA Center for Climate Simulation (NCCS) at Goddard Space Flight Center.

Charlesworth, E., Plöger, F., Birner, T., Baikhadzhaev, R., Abalos, M., Abraham, N. L., et al. (2023). Stratospheric water vapor affecting atmospheric circulation. *Nature Communications*, *14*(1), 3925. https://doi.org/10.1038/s41467-023-39559-2

Chen, J.-J., Swart, N. C., Beadling, R., Cheng, X., Hattermann, T., Jüling, A., et al. (2023). Reduced deep convection and bottom water formation due to Antarctic meltwater in a multi-model ensemble. *Geophysical Research Letters*, *50*(24), e2023GL106492. https://doi.org/10.1029/2023GL106492

Danabasoglu, G., Lamarque, J.-F., Bacmeister, J., Bailey, D. A., DuVivier, A. K., Edwards, J., et al. (2020). The community earth system model version 2 (CESM2). *Journal of Advances in Modeling Earth Systems*, *12*, e2019MS001916. https://doi.org/10.1029/2019MS001916

de F. Forster, P. M., & Shine, K. P. (1999). Stratospheric water vapour changes as a possible contributor to observed stratospheric cooling. *Geophysical Research Letters*, *26*(21), 3309–3312. https://doi.org/10.1029/1999GL010487

Dessler, A. E., Schoeberl, M. R., Wang, T., Davis, S. M., & Rosenlof, K. H. (2013). Stratospheric water vapor feedback. *Proceedings of the National Academy of Sciences*, *110*(45), 18087–18091. https://doi.org/10.1073/pnas.1310344110

Dong, Y., Pauling, A. G., Sadai, S., & Armour, K. C. (2022). Antarctic ice-sheet meltwater reduces transient warming and climate sensitivity through the sea-surface temperature pattern effect. *Geophysical Research Letters*, *49*(24), e2022GL101249. https://doi.org/10.1029/2022GL101249

Dunne, J. P., Horowitz, L. W., Adcroft, A. J., Ginoux, P., Held, I. M., John, J. G., et al. (2020). The GFDL Earth system model version 4.1 (GFDL - ESM 4.1): Overall coupled model description and simulation characteristics journal of advances in modeling Earth systems. *Journal of Advances in Modeling Earth Systems*, *12*(11), 1–56. https://doi.org/10.1029/2019MS002015

England, M., Polvani, L., & Sun, L. (2018). Contrasting the Antarctic and Arctic atmospheric responses to projected sea ice loss in the late twenty-first century. *Journal of Climate*, *31*(16), 6353–6370. https://doi.org/10.1175/JCLI-D-17-0666.1

England, M. R., Polvani, L. M., Sun, L., & Deser, C. (2020). Tropical climate responses to projected Arctic and Antarctic sea-ice loss. *Nature Geoscience*, *13*(4), 275–281. https://doi.org/10.1038/s41561-020-0546-9

Eyring, V., Bony, S., Meehl, G. A., Senior, C. A., Stevens, B., Stouffer, R. J., & Taylor, K. E. (2016). Overview of the coupled model intercomparison project phase 6 (CMIP6) experimental design and organization. *Geoscientific Model Development*, *9*(5), 1937–1958. https://doi.org/10.5194/gmd-9-1937-2016

Fogwill, C. J., Phipps, S. J., Turney, C. S. M., & Golledge, N. R. (2015). Sensitivity of the Southern Ocean to enhanced regional Antarctic ice sheet meltwater input. *Earth's Future*, *3*(10), 317–329. https://doi.org/10.1002/2015EF000306

Fyke, J., Sergienko, O., Löfverström, M., Price, S., & Lenaerts, J. T. M. (2018). An overview of interactions and feedbacks between ice sheets and the Earth system. *Reviews of Geophysics*, *56*(2), 361–408. https://doi.org/10.1029/2018RG000600

Golledge, N. R., Keller, E. D., Gomez, N., Naughten, K. A., Bernales, J., Trusel, L. D., & Edwards, T. L. (2019). Global environmental consequences of twenty-first-century ice-sheet melt. *Nature*, *566*(7742), 65–72. https://doi.org/10.1038/s41586-019-0889-9

Grise, K. M., & Polvani, L. M. (2017). Understanding the time scales of the tropospheric circulation response to abrupt CO2 forcing in the southern hemisphere: Seasonality and the role of the stratosphere. *Journal of Climate*, *30*(21), 8497–8515. https://doi.org/10.1175/JCLI-D-16-0849.1

Held, I. M., Guo, H., Adcroft, A., Dunne, J. P., Horowitz, L. W., Krasting, J., et al. (2019). Structure and performance of GFDL's CM4. 0 climate. *Model Journal of Advances in Modeling Earth Systems*, *11*(11), 3691–3727. https://doi.org/10.1029/2019MS001829

Holton, J. R., Haynes, P. H., McIntyre, M. E., Douglass, A. R., Rood, R. B., & Pfister, L. (1995). Stratosphere-troposphere exchange. *Reviews of Geophysics*, *33*(4), 403–439. https://doi.org/10.1029/95RG02097

Huang, Y., Zhang, M., Xia, Y., Hu, Y., & Son, S.-W. (2016). Is there stratospheric radiative feedback in global warming simulations? *Climate Dynamics*, *46*(1–2), 177–186. https://doi.org/10.1007/s00382-015-2577-2

Inness, A., Chabrillat, S., Flemming, J., Huijnen, V., Langenrock, B., Nicolas, J., et al. (2020). Exceptionally low Arctic stratospheric ozone in spring 2020 as seen in the CAMS reanalysis. *Journal of Geophysical Research: Atmospheres*, *125*(23), e2020JD033563. https://doi.org/10.1029/2020JD033563

Jeong, H., Asay-Davis, X. S., Turner, A. K., Comeau, D. S., Price, S. F., Abernathey, R. P., et al. (2020). Impacts of ice-shelf melting on water-mass transformation in the Southern Ocean from E3SM simulations. *Journal of Climate*, *33*(13), 5787–5807. https://doi.org/10.1175/JCLI-D-19-0683.1

Kang, S. M., Yu, Y., Deser, C., Zhang, X., Kang, I.-S., Lee, S.-S., et al. (2023). Global impacts of recent Southern Ocean cooling. *Proceedings of the National Academy of Sciences*, *120*(30), e2300881120. https://doi.org/10.1073/pnas.2300881120

Kelley, M., Schmidt, G. A., Nazarenko, L. S., Bauer, S. E., Ruedy, R., Russell, G. L., et al. (2020). GISS-E2.1: Configurations and climatology. *Journal of Advances in Modeling Earth Systems*, *12*(8), e2019MS002025. https://doi.org/10.1029/2019MS002025

Kirkman, C. H., & Bitz, C. M. (2011). The effect of the sea ice freshwater flux on Southern Ocean temperatures in CCSM3: Deep-ocean warming and delayed surface warming. *Journal of Climate*, *24*(9), 2224–2237. https://doi.org/10.1175/2010JCLI3625.1

Kuhlbrodt, T., Jones, C. G., Sellar, A., Storkey, D., Blockley, E., Stringer, M., et al. (2018). The low-resolution version of HadGEM3 GC3. 1: Development and evaluation for global climate. *Journal of Advances in Modeling Earth Systems*, *10*(11), 2865–2888. https://doi.org/10.1029/2018MS001370

Levermann, A., Clark, P. U., Marzeion, B., Milne, G. A., Pollard, D., Radic, V., & Robinson, A. (2020). The multimillennial sea-level commitment of global warming. *Proceedings of the National Academy of Sciences*, *110*(34), 13745–13750. https://doi.org/10.1073/pnas.1219414110

Li, D., DeConto, R. M., Pollard, D., & Hu, Y. (2024). Competing climate feedbacks of ice sheet freshwater discharge in a warming world. *Nature Communications*, *15*(1), 5178. https://doi.org/10.1038/s41467-024-49604-3

Li, Q., England, M. H., Hogg, A. M., Rintoul, S. R., & Morrison, A. K. (2023). Abyssal ocean overturning slowdown and warming driven by Antarctic meltwater. *Nature*, *615*(7954), 841–847. https://doi.org/10.1038/s41586-023-05762-w

Lorenz, D. J., & DeWeaver, E. T. (2007). Tropopause height and zonal wind response to global warming in the IPCC scenario integrations. *Journal of Geophysical Research*, *112*(D10), 2006JD008087. https://doi.org/10.1029/2006JD008087

Martin, T., & Xu, X. (2024). Supplementary data for Xu et al. (2025) "Robustness and mechanisms of the atmospheric response over the Southern Ocean to idealized freshwater input around Antarctica [Dataset]. *GEOMAR Helmholtz Centre for Ocean Research Kiel [distributor]*. https://hdl.handle.net/20.500.12085/3351529c-687e-4ac5-bf64-0ce903acf797

Matthes, K., Biastoch, A., Wahl, S., Harlaß, J., Martin, T., Brücher, T., et al. (2020). The flexible ocean and climate infrastructure version 1 (FOCI1): Mean state and variability. *Geoscientific Model Development*, *13*(6), 2533–2568. https://doi.org/10.5194/gmd-13-2533-2020

Maycock, A. C., Joshi, M. M., Shine, K. P., & Scaife, A. A. (2013). The circulation response to idealized changes in stratospheric water vapor. *Journal of Climate*, *26*(2), 545–561. https://doi.org/10.1175/JCLI-D-12-00155.1

Naughten, K. A., Holland, P. R., & De Rydt, J. (2023). Unavoidable future increase in West Antarctic ice-shelf melting over the twenty-first century. *Nature Climate Change*, *13*(11), 1222–1228. https://doi.org/10.1038/s41558-023-01818-x

Newman, P. A., & Nash, E. R. (2000). Quantifying the wave driving of the stratosphere. *Journal of Geophysical Research*, *105*(D10), 12485–12497. https://doi.org/10.1029/1999JD901191

Newman, P. A., Nash, E. R., & Rosenfield, J. E. (2001). What controls the temperature of the Arctic stratosphere during the spring? *Journal of Geophysical Research*, *106*(D17), 19999–20010. https://doi.org/10.1029/2000JD000061

Paolo, F. S., Fricker, H. A., & Padman, L. (2015). Volume loss from Antarctic ice shelves is accelerating. *Science*, *348*(6232), 327–331. https://doi.org/10.1126/science.aaa0940

Park, W., & Latif, M. (2019). Ensemble global warming simulations with idealized Antarctic meltwater input. *Climate Dynamics*, *52*(5–6), 3223–3239. https://doi.org/10.1007/s00382-018-4319-8

Pauling, A. G., Bitz, C. M., Smith, I. J., & Langhorne, P. J. (2016). The response of the Southern Ocean and Antarctic sea ice to freshwater from ice shelves in an Earth system model. *Journal of Climate*, *29*(5), 1655–1672. https://doi.org/10.1175/JCLI-D-15-0501.1

Polvani, L. M., & Waugh, D. W. (2004). Upward wave activity flux as a precursor to extreme stratospheric events and subsequent anomalous surface weather regimes. *Journal of Climate*, *17*, 3548–3554. https://doi.org/10.1175/1520-0442(2004)017<3548>2.0.CO;2

Poshyvailo-Strube, L., Müller, R., Fueglistaler, S., Hegglin, M. I., Laube, J. C., Volk, C. M., & Ploeger, F. (2022). How can Brewer–Dobson circulation trends be estimated from changes in stratospheric water vapour and methane? *Atmospheric Chemistry and Physics*, *22*(15), 9895–9914. https://doi.org/10.5194/acp-22-9895-2022

Purich, A., & England, M. H. (2023). Projected impacts of Antarctic meltwater anomalies over the twenty-first century. *Journal of Climate*, *36*(8), 2703–2719. https://doi.org/10.1175/JCLI-D-22-0457.1

Randel, W. J., Wu, F., & Stolarski, R. (2002). Changes in column ozone correlated with the stratospheric EP flux. *Journal of the Meteorological Society of Japan. Ser. II*, *80*(4B), 849–862. https://doi.org/10.2151/jmsj.80.849

Rye, C. D., Marshall, J., Kelley, M., Russell, G., Nazarenko, L. S., Kostov, Y., et al. (2020). Antarctic glacial melt as a driver of recent Southern Ocean climate trends. *Geophysical Research Letters*, *47*(11), e2019GL086892. https://doi.org/10.1029/2019GL086892

Sadai, S., Condron, A., DeConto, R., & Pollard, D. (2020). Future climate response to Antarctic Ice Sheet melt caused by anthropogenic warming. *Science Advances*, *6*(39), eaaz1169. https://doi.org/10.1126/sciadv.aaz1169

Safieddine, S., Bouillon, M., Paracho, A., Jumelet, J., Tencé, F., Pazmino, A., et al. (2020). Antarctic ozone enhancement during the 2019 sudden stratospheric warming event. *Geophysical Research Letters*, *47*(14), e2020GL087810. https://doi.org/10.1029/2020GL087810

Santer, B. D., Sausen, R., Wigley, T. M. L., Boyle, J. S., AchutaRao, K., Doutriaux, C., et al. (2003). Behavior of tropopause height and atmospheric temperature in models, reanalyses, and observations: Decadal changes. *Journal of Geophysical Research*, *108*(D1), 4002. https://doi.org/10.1029/2002JD002258

Seland, Ø., Bentsen, M., Olivié, D., Toniazzo, T., Gjermundsen, A., Graff, L. S., et al. (2020). Overview of the Norwegian Earth System Model (NorESM2) and key climate response of CMIP6 DECK, historical, and scenario simulations. *Geoscientific Model Development*, *13*(12), 6165–6200. https://doi.org/10.5194/gmd-13-6165-2020

Shindell, D. T. (2001). Climate and ozone response to increased stratospheric water vapor. *Geophysical Research Letters*, *28*(8), 1551–1554. https://doi.org/10.1029/1999GL011197

Siahaan, A., Smith, R. S., Holland, P. R., Jenkins, A., Gregory, J. M., Lee, V., et al. (2022). The Antarctic contribution to 21st-century sea-level rise predicted by the UK Earth System Model with an interactive ice sheet. *The Cryosphere*, *16*(10), 4053–4086. https://doi.org/10.5194/tc-16-4053-2022

Smith, B., Fricker, H. A., Gardner, A. S., Medley, B., Nilsson, J., Paolo, F. S., et al. (2020). Pervasive ice sheet mass loss reflects competing ocean and atmosphere processes. *Science*, *368*(6496), 1239–1242. https://doi.org/10.1126/science.aaz5845

Smith, D. M., Dunstone, N. J., Scaife, A. A., Fiedler, E. K., Copsey, D., & Hardiman, S. C. (2017). Atmospheric response to Arctic and Antarctic sea ice: The importance of ocean-atmosphere coupling and the background state. *Journal of Climate*, *30*(12), 4547–4565. https://doi.org/10.1175/JCLI-D-16-0564.1

Smith, R. S., Mathiot, P., Siahaan, A., Lee, V., Cornford, S. L., Gregory, J. M., et al. (2021). Coupling the U.K. Earth System Model to dynamic models of the Greenland and Antarctic ice sheets. *Journal of Advances in Modeling Earth Systems*, *13*(10), e2021MS002520. https://doi.org/10.1029/2021MS002520

Solomon, S. (1999). Stratospheric ozone depletion: A review of concepts and history. *Reviews of Geophysics*, *37*(3), 275–316. https://doi.org/10.1029/1999RG900008

Stolarski, R. S., McPeters, R. D., & Newman, P. A. (2005). The ozone hole of 2002 as measured by TOMS. *Journal of the Atmospheric Sciences*, *62*(3), 716–720. https://doi.org/10.1175/JAS-3338.1

Stouffer, R. J., Seidov, D., & Haupt, B. J. (2007). Climate response to external sources of freshwater: North Atlantic versus the Southern Ocean. *Journal of Climate*, *20*(3), 436–448. https://doi.org/10.1175/JCLI4015.1

Swart, N. C., Cole, J. N., Kharin, V. V., Lazare, M., Scinocca, J. F., Gillett, N. P., et al. (2019). The Canadian earth system model version 5 (CanESM5. 0.3). *Geoscientific Model Development*, *12*(11), 4823–4873. https://doi.org/10.5194/gmd-12-4823-2019

Swart, N. C., Martin, T., Beadling, R., Chen, J. J., Danek, C., England, M. H., et al. (2023). The Southern Ocean Freshwater input from Antarctica (SOFIA) initiative: Scientific objectives and experimental design. *Geoscientific Model Development*, *16*(24), 7289–7309. https://doi.org/10.5194/gmd-16-7289-2023

Wang, Y., & Huang, Y. (2020). Stratospheric radiative feedback limited by the tropospheric influence in global warming. *Climate Dynamics*, *55*(9–10), 2343–2350. https://doi.org/10.1007/s00382-020-05390-4

Wood, T., McKenna, C. M., Chrysanthou, A., & Maycock, A. C. (2021). Role of sea surface temperature patterns for the Southern Hemisphere jet stream response to CO2 forcing. *Environmental Research Letters*, *16*(1), 014020. https://doi.org/10.1088/1748-9326/abce27

World Meteorological Organization (WMO). (1957). Definition of the tropopause. *World Meteorological Organization Bulletin*, *6*, 136.

Zhu, Z., Liu, J., Song, M., & Hu, Y. (2023). Changes in extreme temperature and precipitation over the southern extratropical continents in response to Antarctic sea ice loss. *Journal of Climate*, *36*(14), 4755–4775. https://doi.org/10.1175/JCLI-D-22-0577.1

Zhu, Z., Liu, J., Song, M., Wang, S., & Hu, Y. (2021). Impacts of Antarctic sea ice, AMV and IPO on extratropical southern hemisphere climate: A modeling study. *Frontiers in Earth Science*, *9*, 757475. https://doi.org/10.3389/feart.2021.757475

Ziehn, T., Chamberlain, M. A., Law, R. M., Lenton, A., Bodman, R. W., Dix, M., et al. (2020). The Australian earth system model: ACCESS-ESM1.5. *Journal of Southern Hemisphere Earth Systems Science*, *70*(1), 193–214. https://doi.org/10.1071/ES19035

References From the Supporting Information

Fichefet, T., & Maqueda, M. A. M. (1997). Sensitivity of a global sea ice model to the treatment of ice thermodynamics and dynamics. *Journal of Geophysical Research*, *102*(C6), 12609–12646. https://doi.org/10.1029/97JC00480

Madec, G. (2016). *NEMO ocean engine* (p. 406). Note du Pôle modélisation de l'Institut Pierre- Simon Laplace No 27.

Reick, C. H., Raddatz, T., Brovkin, V., & Gayler, V. (2013). Representation of natural and anthropogenic land cover change in MPI-ESM. *Journal of Advances in Modeling Earth Systems*, *5*(3), 459–482. https://doi.org/10.1002/jame.20022

Stevens, B., Giorgetta, M., Esch, M., Mauritsen, T., Crueger, T., Rast, S., et al. (2013). Atmospheric component of the MPI-M Earth system model: ECHAM6. *Journal of Advances in Modeling Earth Systems*, *5*(2), 146–172. https://doi.org/10.1002/jame.20015

Valcke, S. (2013). The OASIS3 coupler: A European climate modelling community software. *Geoscientific Model Development*, *6*(2), 373–388. https://doi.org/10.5194/gmd-6-373-2013

Zeller, M., & Martin, T. (2024). On warm bias and mesoscale dynamics setting the Southern Ocean large-scale circulation mean state. *Ocean Modelling*, *191*, 102426. https://doi.org/10.1016/j.ocemod.2024.102426